We are IntechOpen, the world's leading publisher of Open Access books Built by scientists, for scientists

4,800
Open access books available

122,000
International authors and editors

135M
Downloads

Our authors are among the

154
Countries delivered to

TOP 1%
most cited scientists

12.2%
Contributors from top 500 universities

CLARIVATE ANALYTICS BOOK CITATION INDEX INDEXED

WEB OF SCIENCE™

Selection of our books indexed in the Book Citation Index in Web of Science™ Core Collection (BKCI)

Interested in publishing with us?
Contact book.department@intechopen.com

Numbers displayed above are based on latest data collected.
For more information visit www.intechopen.com

10

Mine Detection Robot and Related Technologies for Humanitarian Demining

Kenzo Nonami*, Seiji Masunaga*, Daniel Waterman*
Hajime Aoyama**, and Yoshihiro Takada**
*Chiba University
Japan
**Fuji Heavy Industries
Japan

1. Introduction

Currently, more than 100 million anti-personnel mines are under the ground all over the world. These mines not only disturb the economic development of mine-buried nations, but also injure or kill more than 2000 people a month. As a result, the removal of landmines has become a global emergency. The current method of removing mines manually is costly and dangerous. Moreover, removal of all mines by this method would require several hundred years (it would takes one thousand according to a CMAC report based on Cambodian Mine Action Center Current Activities 1998), during which time, more mines might be buried in war zones.

There are three kinds of demining strategies. The first is human deminier based demining. The second is mechanical equipment based demining like Fig.1(Geneva International Center for Humanitarian Demining,2002). The third is advanced robot based demining. Currently, the most common demining approach is the first type. The second type is applied in some limited mine field area. The third type is partially tried as mine detection or brush cutting with the exception of research oriented robots and some of them will be expected in future demining approaches. Figure 2 shows the robotic brush cutter which was developed in the Demining Technology Workshop in Cambodia. This robot can cut grass and bush by teleoperation.

Figure 3 shows the four legged mine detection robot which was studied by CSIC-IAI, Spain in 1999(Armada et al.2005). Under this extreme environment, a walking robot may be an effective and efficient means of detecting and removing mines while ensuring the safety of local residents and people engaged in the removal work. The six-legged and crawler type hybrid robot COMET-III(Nonami et al.2003) shown in Fig.4 with two manipulators based on the added stability, mobility, and functionality that this platform offers. This latest robot COMET-III, which is fully autonomous, has been developed by one of this paper's authors.

Source: Humanitarian Demining: Innovative Solutions and the Challenges of Technology, Book edited by: Maki K. Habib, ISBN 978-3-902613-11-0, pp. 392, February 2008, I-Tech Education and Publishing, Vienna, Austria

Fig. 1. Mechanical demining equipment

Fig. 2. Tempest for brush cutter

Fig. 3. Four legged mine detection robot

Fig. 4. Mine detection robot COMET-III

The total weight is about 1000kg, the size is 4m long, 2.5m wide, and 0.8m high. The COMET-III has 40 litter gasoline tank to continuously work for 4 hours and 700cc gasoline engine like an automobile engine to generate DC power supply and to drive the hydraulic motor. So, the driving force is based on hydraulic power with 14 MPa high pressure and the total power is 25PS. The walking speed on six legs is about 300m/h and the running speed by rubber crawler is 4km/h. Therefore, the COMET-III is a hybrid system and it has two manipulators which are used for mine detection and marking. Also it has a 3D stereo vision camera to make online mapping and trajectory planning, so the COMET-III can be called a fully autonomous mine detection robot. This kind of robot is the third type of demining strategy, based on advanced robotics, and is the future's approach.

Currently our group is participating in the Japan Science and Technology Agency's (JST) Sensing and Access Control R&D for Humanitarian Mine Action project with our effort to develop a small vehicle for mine detection and clearance. This small vehicle is named Mine Hunter Vehicle(MHV). Specifically we were concerned with the development of a 4 degree-of-freedom robot arm which is called as SCARA arm for sensing buried anti-personnel mines. We have divided the project into several tasks to be tackled. Our team, in cooperation with Fuji Heavy Industries and Sato's group from Tohoku University, and Arai's group from University of Electro-Communications has proposed a small teleoperated vehicle-based system. The task of landmine detection is being undertaken by Sato's group at Tohoku University, who are developing an array-style ground penetrating radar (SAR-

GPR). Our group including Fuji Heavy Industries is responsible for the development and control of an arm that the sensor will be mounted on and the mine clearance manipulator.

2. State of the art of Teleoperated Mine Detection by Vehicle Mounted Mine Detector

Conventional vehicle-mounted mine detector systems employ an array of sensors elements to achieve a detection swath typically 2~4m wide. Some systems employ more than one type of sensor technology. These systems, while being very useful are often expensive, complex and inflexible. A human operator, on the other hand, sweeps a mine detector from side to side while moving forward to cover ground. The operator can follow the ground profile with the detector head close to the ground without hitting the ground or any objects on it. The operator can also vary the wide of sweep to suit a particular situation, and is usually not limited by terrain. However the manual method is slow, harzardous, manpower-intensive, and stressful to the operation who, as a result, can perform this task only for short periods at a time. As well, the task is monotonous and at times errors result due to operator inattentiveness.

Canadian Center for Mine Action Technologies (CCMAT) developed the robotic scanner shown in Fig.5 which uses a robotic device capable of autonomously moving a mine detection sensor over natural ground surfaces including roads and tracks in a manner similar to a human operator. Such a device, operated remotely, will increase the safety of the personnel performing mine detection. As well, this will provide a more flexible and less expensive way of sweeping surfaces such as roads and fields than systems which employ a static array of a vehicle-mounted systems. Although several vehicle-mounted systems are protected against conventional antitank mines, they still may require a precursor vehicle to neutralize antipersonnel and tilt-rod mines. For the system proposed by CCMAT, the requirement for protection will be much reduced primarily because mines will be detected ahead of the vehicle without the sensor contacting the ground.

Figure 6 shows the vehicle mounted mine detector (VMMD). The VMMD is a modified small utility vehicle. The VMMD sensor package consists of Ground Penetrating Radar (GPR) and infrared and ultraviolet cameras. The VMMD did well in detecting antitank mines, but had difficulty identifying antipersonnel mines and proved very complicated to operate.

Figure 7 shows the semi-autonomous mine detection system (SAMS). The SAMS is designed to reduce the threat to deminers by remotely detecting, marking and allows towing of a Sciebel Metal Detection Array. SAMS can remotely navigate into minefields to detect, mark,and map buried mines using a metal detection array and differential GPS position location equipment under semi-autonomous remote control.

Fig. 5. Robotic Scanner mounted on teleoperated vehicle[5]

Fig. 6. Vehicle Mine Detector (VMMD)[6]

Figure 8 shows another Vehicle Mounted Detection System (VMDS). The VMDS concept is based on a commercial skid steer chassis modified to incorporate a remote control capability. The VMDS sensor package consists of a 2m wide Sciebel metal detection array, a Thermal-Neutron Analysis (TNA) sensor, and an infrared sensor. The 2meter array detects metal objects in the vehicle's path, while the TNA indicates those targets that contain explosive. In testing, the 2meter detection array performed extremely well. The TNA found most AT mines, but had difficulty identifying AP mines and proved very complicated to operate.

3. Concept and Implementation of Mine Hunter Vehicle (MHV)

As above mentioned, our group was participating in the JST Sensing and Access Control R&D for Humanitarian Mine Action project with our effort to develop a small vehicle for mine detection and clearance. This small vehicle is named Mine Hunter Vehicle (MHV) and is equipped with mine detection sensors. The general design considerations were as follows;

(1) A robot that can be loaded into 2 ton vehicles.
(2) Division is easy.
(3) The weight of the main part of the vehicles is 1100kg - 1500kg.
(4) It has an environment-proof nature, able to carry out a certain operation in the climate of Afghanistan.
(5)The vehicle can climb up and down slopes in mountain regions.
(6)The vehicle has durability against blasts from antipersonnel mines.
(7)A reliable control device should be developed.
(8)Both front detection and side detection are possible.

The design specification of the main body of MHV was as follows;

(1) Simple body structure
(2)45-degree slope climbing capability, and spin turn.
(3)Durability and reliability test of an engine system, a drive system, and axle part
(4)Development of the axle which can easily fitted with crawlers or tires
(5)Durability and reliability test of bulletproof equipment of an anti-personnel mine level

(6)Durability and reliability test of the protection-against-dust nature which prevents invasion of minute sand etc. into flexible regions
(7)Development of a reliable controller, a remote control, and image transmission equipment

The body full length of MHV is 2.8m, and when the sensor arm is lengthened, it is 4.5m. The width of vehicle is 1.5m in the case of crawler, and is 1.6m in the tire. The height of vehicles is 1.9m in the crawler, and is 1.8m in the tire. The full weight is 1650kg including SCARA arm. The drive is a diesel engine and a HST (Hydraulic Static Transmission) system. Four independent crawlers are attached to the front right, the front left, the back right, and the back left. The engine was selected to be applicable to the 2,000m high elevation in Afghanistan. The left-hand side crawler (front, rear) and right-hand side crawler (front, rear) have a separate hydraulic pump and the hydraulic circuits are independent of each other. Furthermore, MHV crawlers can rotate in ±25 degrees centering on an axle. Because of this reason, the slip of the crawlers on road surfaces decreased and it became easier to negotiate irregular ground and ascend and descend sloped ground. Changing between crawlers and tires can be down easily by removing eight bolts, like changing a tire of a normal car. A high-strength steel plate of 4.5mm was attached in front with the bolts. The rotation part of the axles are bush bearings strong against shock and do not require lubirication, however in order to prevent sand and dust from invading the bearings, oil seals are attached to both sides. Even if the axles are submerged in water, there will be no leak.
The control device consists of modules which include the controller for hydraulic pressure, a proportionality electromagnetic valve driver, a remote control, image transmission equipment, manipulator control equipment and the controller equipment of a mine detection sensor. In failure, in consideration of maintenance nature, correspondence was made possible by module provision. The body became heavier as a result of strengthening, better waterproofing, protection against dust, and bulletproofing. As a result, the target weight limit was set to 1,600kg. The engine power is 39PS, and the hydraulic pressure is 180kg/cm^2

The design specification of the sensor arm of MHV is as follows;
(1) In order to secure horizontal accuracy of position for a wide working range, a horizontal SCARA (Selective Compliance Assembly Robot Arm) robot arm with multiple joints was adopted.
(2) Reduction gears were made into the plunocent rucksack system instead of a harmonic drive to minimize vibration.
(3) The sensor arm itself has a waterproof level of IP30. For this reason, the whole arm was dressed with the jacket and waterproofing and protection against dust were secured.
(4) In order to always keep the direction of a mine detection sensor constant, a timing belt was used to move a joint in synchronization with the rotation of the arm..
(5) The SCARA arm has four-degeree-of-freedom. Two-degree-of-freedom are horizontal, one is the perpendicular, and one is the yaw of the sensor. Also they are driven by AC servo motors.
(6) The maximum payload is 40kg. Each arm length is 80cm. The maximum speed at a tip

is 10 m/min and repetition positioning accuracy is ±1mm in the horizontal direction and ±1mm in the perpendicular direction.

(7) The maximum payload size is 400mm x 400mm x 400mm, and the SCARA arm full weight is 150kg.

(8) GPR and a metal detector are installed at the tip of the SCARA arm, with gap control used for the metal detector and gap control used for the GPR.

The system consists of three parts which are control for the main body of MHV, SCARA arm control, and the mine detection sensor. Figures 7 and 8 show the field test in Sakaide city, Kagawa prefecture in March,2006. Also, the performance of MHV was carried out in March, 2007, Croatia.

Fig. 7. Mine Hunter Vehicle with two manipulator

Fig. 8. Mine detection test of MHV

After this, the controlled metal detector installation schedule on MHV is explained in detail. And then, the current state of development in the anti-personnel mine exposure and clearance system is described, focusing on the robot arm. In particular, we have achieved the reasonable performance of a 6-degree of freedom robot with multi-function tool by means of nonlinear control based on "LOOK AT TABLE" scheme or control theory scheme and also the master-slave hand.

4. Controlled Metal Detector Mounted on Mine Detection Robot

4.1 Overview

Metal detectors are considered as the most reliable sensors for mine detection work. However, landmine detection performance of the metal detectors is highly dependent on the distance between the sensor heads and the buried landmines. Therefore, the landmine detection performance of the metal detectors could be substantially improved if the gap and attitude of the sensor heads can be controlled. In case of robots assisted land mine detection, this function can be performed in a convenient manner where the sensor heads should accurately follow the ground surface maintaining almost uniform gap between the ground surface and the sensor heads by controlling the gap and attitude of the sensor heads. Few mine detection robots that have the capability to recognize ground surface and can control

the gap and attitude of the sensor heads are reported in (Armada, M.A. et al. 2005), (Chesney, R. et al. 2002), (Nonami, K. et al. 2003).
However, to the best of the knowledge of the authors, no research work has been reported in the literature that quantitatively addressed the relationship between the landmine detection performance and controlling the gap and attitude of the sensor head to the ground surface.
The CMD system adopts 3-D stereovision camera rather than LASER scanning as a range sensor because 3-D stereovision camera can capture color information also. Ground of real minefield may have substantial amount of vegetation. Therefore, some image-processing algorithm could be applied with the color images captured by the CCD cameras for recognition of the vegetation to autonomous operation of the CMD in vegetated minefield in future work.
The trajectories are generated by the CMD in such a manner that any obstacle or possible impact with the ground can be avoided. The CMD then tracks the generated trajectories by a trajectory-tracking controller so that the sensor head can follow the ground surface. The effectiveness and the impact related to the gap and attitude control on the mine detection performance of the CMD have been demonstrated by experimental studies.
The rest of the paper is organized as follows. The description of the controlled object has been presented in section 4.2. The kinematic analysis of the CMD has been presented in section 4.3. The description of stereovision camera has been presented in section 4.4. The description of trajectory planning has been presented in section 4.5. The results of experiments of trajectory tracking have been presented in section 4.6. The results of experiments of mine detection have been presented in section 4.7, 4.8. The some conclusions have been presented in section 4.9.
In view of the above, authors' research group has developed a Controlled Metal Detector (CMD) having 3-DOF for any arbitrary positioning of the sensor head. The CMD system can generate 3-D high-speed mapping of the ground surface and can generate trajectories of the sensor head with 3-D stereovision camera. 3-D stereo vision is now being widely used for 3-D mapping and robotics (Clark, F. et al. 2007), (Rochaa, R. et al. 2005), (Xiao, D., et al. 2004) for their powerful sensing capability than other range sensors.

4.2 Controlled Object

The controlled object of this research is called Controlled Metal Detector (CMD). It consists of the two-coil metal detector and a 3-DOF mechanical manipulation mechanism driven by electric motors. The overview of the CMD system is shown in Fig.9. The experimental setup is composed of the main body of the CMD, two PCs, 3-D stereovision camera and a XY-stage as shown in Fig.10. The XY-stage *can perform* the two-dimensional motion in horizontal directions.
The schematic diagram of the CMD is shown in Fig.11. The CMD has 3-DOF composed of three motorized linkages (Link 1, Link 2, and Link 3). The ball screws on these links convert the rotational motion into translation motion. The gyrations of pitch and roll, and movement in vertical direction of the sensor head are performed by controlling the lengths of the Link 1, Link 2 and Link 3. The right-handed coordinate system $\{O_b\ X_b\ Y_b\ Z_b\}$ associated with the CMD is described in Fig.11. The lengths l_1, l_2 and l_3 (of Link 1, Link 2 and Link 3 respectively) are measured with encoders installed in each link. The calculation methods are described in next section.

The CMD is mounted on the horizontal positioning arm of the XY-stage at the point P_a. Therefore, the point P_a does not move vertically. After the synchronization of the CMD and the horizontal positioning arm of the XY-stage, it is possible to make the sensor head to follow the target trajectories generated with 3-D stereovision data. Moreover, the CMD has no metallic parts within 600 mm from the sensor head; this practically eliminates any chance of interference on the metal detector. Table 1 shows the specifications of the CMD.

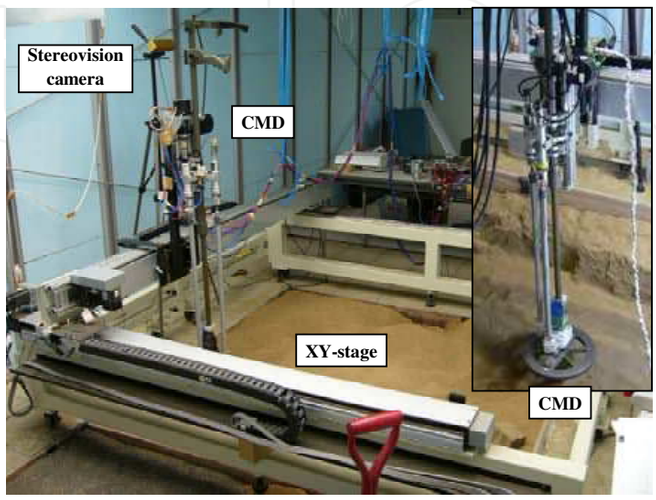

Fig. 9. Overview of CMD system

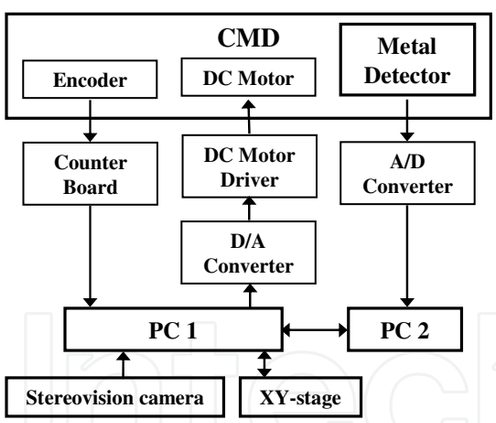

Fig. 10. Architecture of CMD system

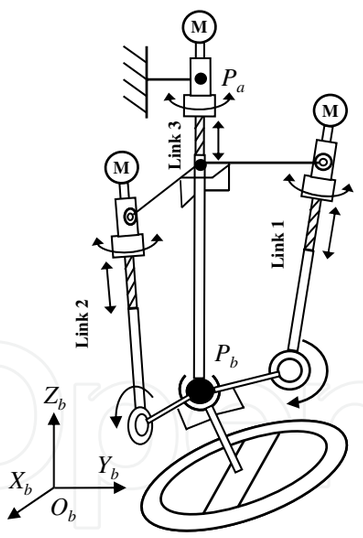

Fig. 11. Configuration of CMD

4.3 Kinematic Analysis

The movements of Link 1 and Link 2 are restrained in the perpendicular plane because there is a ditch on the ball joint P_b. The geometrical relationship between the lengths l_1, l_2 and the

Item	Value	Remarks
Length [mm]	1500	Basic position
Width [mm]	282	
Weight [kg]	10	
Degree of freedom	3	
Stroke speed (max) [mm/s]	100	Link 3
Stroke width [mm]	180	Link 3
Angular velocity (max) [deg/s]	10	Pitch, Roll
Angle range [deg]	± 15	Pitch, Roll
Length of l_4 [mm]	835	
Length of l_5 [mm]	80	

Table 1. Specifications of CMD

pitch angle θ_x, roll angle θ_y of the sensor head shown in Fig. 12 In the CMD system, in order to ensure that the sensor head follows the ground surface without any collision, the trajectory of the attitude of the sensor head and the required change in l_3 are calculated with 3-D vision data. Then the changes in lengths l_1, l_2 are calculated from the inverse kinematics as shown below (1) and (2).

$$l_1 = \sqrt{{l_4}^2 + 2{l_5}^2 - 2l_5 L\sin(\theta_x + \arctan\frac{l_5}{l_4})} - l_4 \tag{1}$$

$$l_2 = \sqrt{{l_4}^2 + 2{l_5}^2 + 2l_5 L\sin(\theta_y - \arctan\frac{l_5}{l_4})} - l_4 \tag{2}$$

Moreover, the direct kinematics is as follows.

$$\theta_x = -\arctan\frac{l_5}{l_4} + \arctan\frac{-{l_1}^2 - 2l_1 l_4 + 2{l_5}^2}{2l_5 L} \tag{3}$$

$$\theta_y = \arctan\frac{l_5}{l_4} + \arctan\frac{{l_2}^2 + 2l_2 l_4 - 2{l_5}^2}{2l_5 L} \tag{4}$$

Where l_4 and l_5 are lengths of links, and $L = \sqrt{{l_4}^2 + {l_5}^2}$. Moreover, attitude vectors $\boldsymbol{X}_s$, $\boldsymbol{Y}_s$ of the sensor head are defined as $\boldsymbol{X}_s = [\cos\theta_y, 0, -\sin\theta_y]^T$, $\boldsymbol{Y}_s = [0, \cos\theta_x, \sin\theta_x]^T$ with attitude angles θ_x, θ_y.

4.4 Ground Mapping with 3-D Stereo Vision

The commercial stereovision camera, called Bumblebee (Point Grey Research Inc.), has been used for 3-D stereovision based ground mapping. This stereovision camera uses a parallel stereo method. Table 2 shows the specifications of the stereovision camera. Where the coordinate system consists of: the original point and the Z_c axis are taken the optical center and the optical axis of the left camera, the X_c axis and the Y_c axis are taken the horizontal axis and the vertical axis of the left image, is defined as the camera coordinate system $\{O_c\}$.

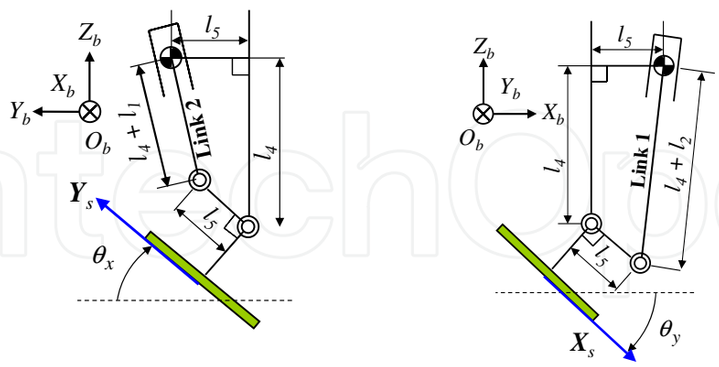

(a) Pitch of CMD (b) Roll of CMD

Fig. 12. Geometry of CMD

The stereovision algorithm searches for correspondence points between the left image and the right image acquired with the stereovision camera by the template match. The camera coordinate $[x_c, y_c, z_c]^T$ of point P in the 3-D space is decided from correspondence points p, p' in the right and left images as follows.

$$x_c = \frac{x_l B}{x_l - x_r}, y_c = \frac{y_l B}{x_l - x_r}, z_c = \frac{fB}{x_l - x_r} \tag{5}$$

Where the positions of correspondence points p and p' on the right and left images are defined as (x_l, y_l), (x_r, y_r).

As a result, geographical features information in the camera coordinate system is acquired. Therefore, depth information $f_a(x, y)$ on the ground surface in the base coordinate system is generated with the coordinate conversion. Here a photograph of the detection area as an example is shown in Fig. 13, and the 3-D geographical features map is shown in Fig. 14.

Item	Value
Device size [mm]	160(W)×40(H)×50(D)
Weight [g]	375
Baseline [mm]	120
Focal length [mm]	6
Pixels	320(H) × 240(V)
view angle [deg]	50

Table 2. Specifications of stereovision camera

Fig. 13. Detection area

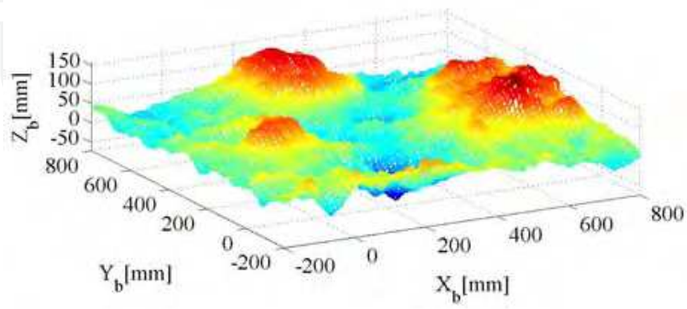

Fig. 14. 3-D mapping

4.5 Trajectory Planning with 3-D Vision Data

The trajectory planning is produced by the off-line. Namely, at first, the 3-dimensional map for the detection area like 1m × 1m will be produced by means of the stereovision based image processing, and then, the trajectory planning will be automatically done. The target trajectory has been generated from the depth information acquired with 3-D stereovision. However, the raw depth information from the stereovision camera contains large data volume and also noise. This large volume of data is inconvenient for the trajectory planning. Therefore, a working depth information $f(n_1, n_2)$ has been generated from the original depth information $f_a(x, y)$ provided by the stereovision camera after sampling it at a grid interval d_g. Thus, the working depth information $f(n_1, n_2)$ can be written as:

$$f(n_1, n_2) = f_a(n_1 d_g, n_2 d_g) \tag{6}$$

Where n_1 and n_2 are assumed integers. This working depth information $f(n_1, n_2)$ on the grid has been used in the trajectory planning algorithm.

Figure 15 shows the trajectory of the mounting point P_a of the CMD on landmine detection area (l_x × l_y). The point P_a moves parallel to the X_b - Y_b axis with velocities v_x and v_y respectively. Here, it is necessary to change the velocities of the point P_a depending on the ground surface. However, during the experiment the velocities v_x and v_y are kept equal because of the technical limitations of the XY-stage.

During the trajectory planning, first the position and attitude angles of the sensor head are decided on each grid point of $f(n_1, n_2)$; then these discrete points in the space are connected by straight lines to generate a continuous trajectory. The following objectives are to be satisfied during the trajectory planning:

1. The sensor head keeps itself approximately parallel to the ground surface.
2. The collision between the sensor head and the ground surface is avoided.

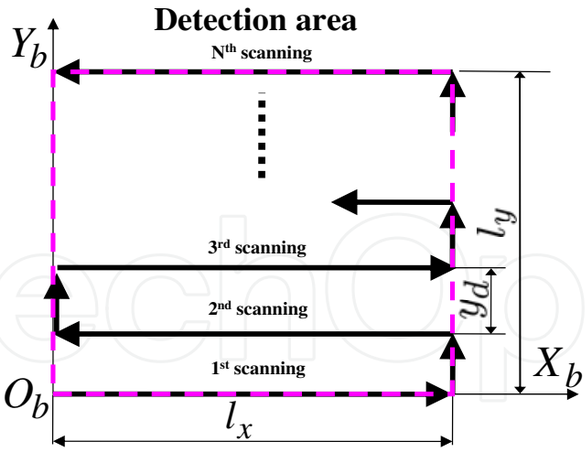

Fig. 15. Trajectory of XY-stage

4.5.1. Decision of Attitude Angles

The target attitude angles θ_x *and* θ_y of the sensor head that fulfill the first objective stated earlier can be obtained from the depth information as the inclinations of the ground surface. The X_b axial inclination at the grid point (n_1, n_2) of the ground surface is decided by the least square method as follows.

$$\theta_y = \frac{n_s \sum_{i=1}^{n_s} x_i z_i - \sum_{i=1}^{n_s} x_i \sum_{i=1}^{n_s} z_i}{n_s \sum_{i=1}^{n_s} x_i^{\,2} - \left(\sum_{i=1}^{n_s} x_i \right)^2} \tag{7}$$

$$\begin{cases} n_s = (2k_s + 1) \\ x_i = n_1 - k_s + i \\ z_i = f(n_1 - k_s + i, n_2) \end{cases} \tag{8}$$

θ_x is similarly decided. Where k_s is defined as an inclination coefficient of determination. However, the target attitude angles are decided in restrictions. One of the restrictions are is the movable ranges of the mechanism. Another one is the limits of attitude movements θ_{dx} and θ_{dy} between each grid point that consider the passing velocity, v_x and v_y, of the point P_a. The limits of the attitude movements θ_{dx} and θ_{dy} are shown below. Where ω_{MAX} shows the maximum angular velocity.

$$\theta_{dx} = \pm \frac{\omega_{MAX} d_g}{v_x}, \theta_{dy} = \pm \frac{\omega_{MAX} d_g}{v_y} \tag{9}$$

4.5.2. Decision of Length of Link 3

Length l_3 of Link 3 that fulfills the second objective stated earlier is decided with the attitude angles. When the position of the point P_a is $\boldsymbol{P}_a = \left[n_1 d_g, n_2 d_g, P_{az} \right]^T$, the position of the center point of the ball joint P_b is $\boldsymbol{P}_b = \left[n_1 d_g, n_2 d_g, P_{az} - d_z - l_3 \right]^T$. Where the fixed height of the point P_a is assumed to be P_{az}. Moreover, the distance between the point P_a and the point P_b in the

basic stance is assumed to be d_z. Where position $\boldsymbol{S}$ at the center point S on the sensor head's bottom is as follows with attitude vectors $\boldsymbol{X}_s$ and $\boldsymbol{Y}_s$ on each grid point.

$$\boldsymbol{S} = l_s \frac{\boldsymbol{Y}_s \times \boldsymbol{X}_s}{\left|\boldsymbol{Y}_s \times \boldsymbol{X}_s\right|} + \boldsymbol{P}_b \tag{10}$$

Where l_s is defined as the distance between the point P_b and the point S. At this time, all the points on the sensor head's bottom keep a distance more than a safety allowance l_{mar} to the ground surface. Therefore maximum length l_3 is decided as filled above. However, l_3 is decided in the restriction of the movable range of the mechanism.

4.5.3. Re-decision of Length of Link 3

Because this trajectory planning targets at minefield, the length l_3 of Link 3 is decided again so that the sensor head does not touch the ground surface in spite of the delay is caused in each response of the Links.

On the i_{th} grid point of the trajectory that XY-stage passes, the position of the point P_a is assumed to be $\boldsymbol{P}_a(i) = \left[n_1(i)d_g, n_2(i)d_g, P_{az}\right]^T$, the pitch angle and the roll angle of the sensor head are assumed to be $\theta_x(i)$, $\theta_y(i)$ and the length of Link 3 is assumed to be $l_3(i)$.

In the present research, the CMD does the following three operations at the same time.

1. Attitude changes of the sensor head
2. Vertical motions of the sensor head
3. X_b and Y_b axial motions by XY-stage

Here the length $l_3(i)$ of Link 3 is decided again so that the CMD safely accommodate the time delay caused by these three operations. Here, these three operations are assumed to be completed by the arrival time d_g/v_x, d_g/v_y to the next grid point.

The length $l_3(i)$ is decided again so that all the points on the sensor head's bottom may keep the gap to the depth information on the grid point more than the safety allowance l_{mar} as shown in Fig. 16, evenif the points P_a is at $\boldsymbol{P}_a(i\text{-}1)$ and $\boldsymbol{P}_a(i\text{+}1)$ with the target attitude angles of the sensor head of the i_{th} grid point. Thus, the collisions with the ground surface caused by the delay of the response can be avoided. However, $l_3(i)$ is decided in the restriction of the movable range of the mechanism and the limits of the expansions l_{dx} and l_{dy} between each grid point that consider the passing velocity, v_x and v_y, of the point P_a. The limits of the expansions l_{dx} and l_{dy} are shown below. Where v_{MAX} is assumed the maximum expansion velocity of Link 3.

$$l_{dx} = \frac{v_{MAX} d_g}{v_x}, l_{dy} = \pm \frac{v_{MAX} d_g}{v_y} \tag{11}$$

Figure 17. shows an example of the generated target trajectory at the center of the sensor head's bottom.

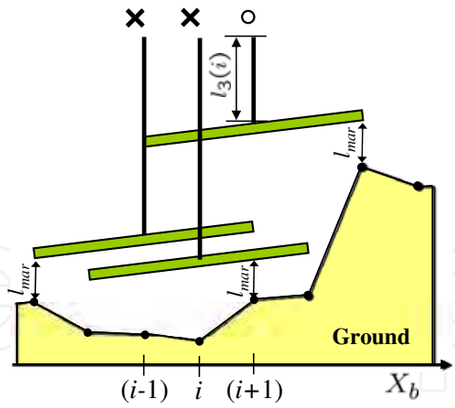

Fig. 16. Decision of l_3

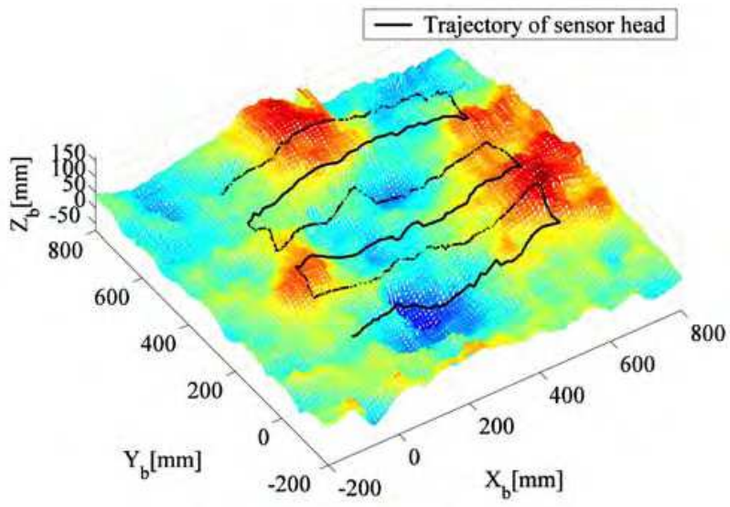

Fig. 17. Trajectory generation

4.6 Experiments of Trajectory Tracking

The trajectory following experiments of the CMD are conducted over the detection area (600 mm × 40 mm) shown in Fig. 18. 3-D range information of the detection area is acquired with the stereovision camera in the experiment and the target trajectory is generated using the methods stated earlier. Here each control input to the motor drivers of the CMD is generated with PID controller of feedback control system so that each expansion of the Links follows to the target trajectory. Where the sampling frequency is taken as 50 Hz. Moreover, each gain of the PID controller is shown in Table 3, and each parameter in the trajectory planning is shown in Table 4.

Fig. 18. Detection area for experiment

Link	P	I	D
Link 1	1.5	2.5	0.01
Link 2	3.0	12.0	0.1
Link 3	3.0	12.0	0.1

Table 4. Parameters of trajectory generation

v_x	v_y	y_d	l_{mar}	d_g	k_s
50mm/s	10mm/s	40mm	10mm	10mm	10

Table 3. Gain of PID controller

4.6.1. Experimental Result

Figure 19 showed the generated target trajectory and the result at the center of the sensor head's bottom in the experiment. Fig. 20 showed the time change of the vertical minimal gap between the sensor head's bottom and the ground surface. Fig. 20 shows not real data, but the final data after signal processing in the PC. In addition, these spike peaks are caused by the discrete data like Fig.16. Moreover, the target trajectory and the response of each expansion of Link 1, Link 2 and Link 3 from the experiment beginning for four seconds are shown in Fig. 21.

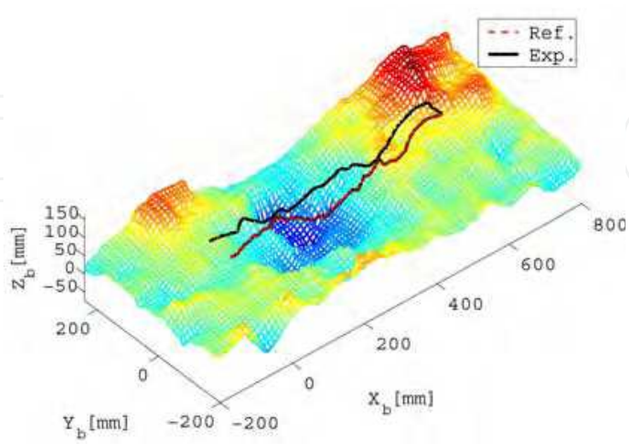

Fig. 19. Trajectory of sensor head

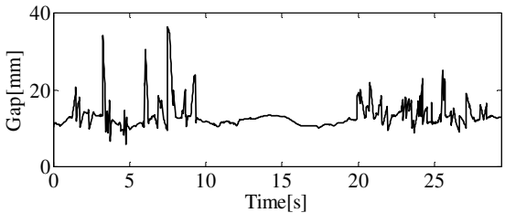

Fig. 20. Gap between sensor head and ground surface

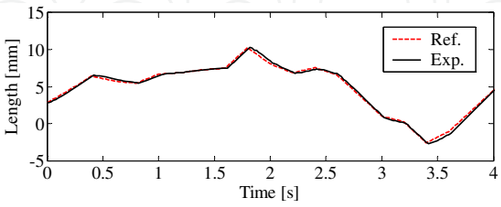

(a) Link 1

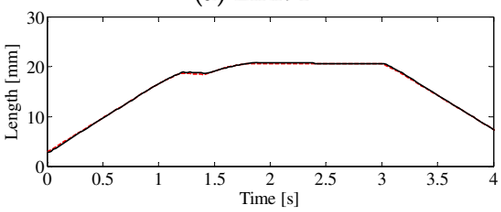

(b) Link 2

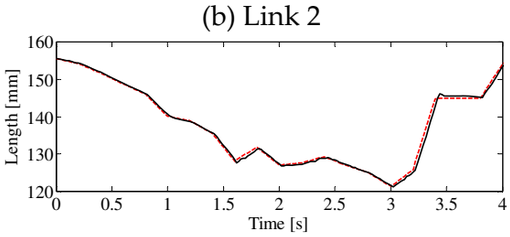

(c) Link 3

Fig. 21. Trajectory responses of links

4.6.2. Consideration

From Fig. 19, it is obvious that the sensor head follows the generated target trajectory very well. In addition, the sensor head almost keeps the gap more than the safety allowance l_{mar} (Fig. 20) during the detection work, and the trajectory that fulfills the target specifications without contact with the ground surface has been achieved. The safety allowance defined as l_{mar} = 10 mm was appropriate in this experiments. Moreover, each link has an excellent trajectory following performance with a small overshoot and delay respectively as shown in Fig. 21.

4.7 Methods of Estimating the Position of Buried Landmines

Estimating the position of the buried landmines with the data of landmine detection sensors is important in detection work by mine detection robots. The metal detector used in this research has a property that the frequency of the output changes before and after the metal

detector mounted on the CMD is passing over a buried metallic object. By using this property, the output signal from the metal detector is converted to a negative value when a landmine exists on the right side from the center of the sensor head along the X_b axis, and to a positive value when a landmine exists on the left side from the center of the sensor head along the X_b axis. The position of the buried landmine is estimated with the processed output of the metal detector.

This section shows the method of estimating the buried position that is confined to the case of the detection area with only one buried landmine. The sensor head is scanned X_b axially in N times in each landmine detection experiment in this research as shown in Fig. 15. In each X_b axially scanning, the strength of the metal reaction: m_i and candidate position of the buried landmine: $[x_i, y_i]$ are decided with the output of the metal detector. After all (N times) scanning finished, the estimated position of the buried landmine is decided with each strength of the metal reaction and each candidate position of the buried landmine as follows.

$$[x, y] = \left[\frac{\sum_{i=1}^{N} m_i x_i}{\sum_{i=1}^{N} m_i}, \frac{\sum_{i=1}^{N} m_i y_i}{\sum_{i=1}^{N} m_i} \right] \tag{12}$$

Where in the i^{th} scanning, the candidate position of the buried landmine $[x_i, y_i]$ is decided as the middle point of the positions in which the metal reactions pass the threshold V_d[V] or -V_d[V] along the X_b axially with keeping the output increases. In addition, the strength of the metal reaction m_i is assumed a difference between the maximum and minimum values in neighborhood at the candidate position as shown in Fig. 22. Where it is assumed that V_d = 0.2 V and N = l_y/y_d + 1 in this research.

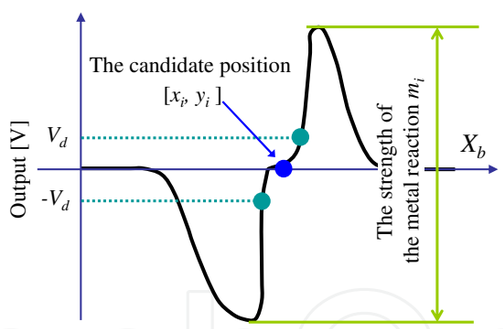

Fig. 22. Definitions of the candidate position (i^{th} scanning)

4.8 Experiments of Mine Detection

Various roughnesses are given to detection area ($l_x \times l_y$) of sands shown in Fig. 18, and the landmine detection experiments by the CMD are conducted. The position of the buried landmine is estimated with acquired data of the metal detector, and effectiveness of the gap and attitude control of the sensor head to landmine detection performance is verified. Here the control method is assumed same to the experiments of trajectory tracking in section 4.6.

4.8.1. Experimental Conditions

Three kinds of trajectories are defined in this experiment to verify effectiveness of the gap and attitude control to landmine detection performance and they are compared. Where Case

1 is a target trajectory that fixes the sensor's posture horizontally with keeping the safety allowance l_{mar} to the highest point of the detection area. Case 2 is a target trajectory that fixes the sensor's posture horizontally, and controls only the gap between the sensor head and the ground surface. Case 3 is a proposed target trajectory that controls the gap and attitude of the sensor head to the ground surface.

The buried landmines are the mostly antipersonnel landmines all over the world, PMN2 (125 mm × 54 mm), made of plastic in Fig. 23 (a) and have some metallic parts. Depths of the buried landmines are defined as the distance between the ground surface and the upper surface of the landmines as shown in Fig. 23 (b). In addition, the buried position was assumed to be [x, y] = [300 mm, 300 mm] on base coordinate system.

About conditions concerning the ground surface, a smooth ground surface is defined as area A, the ground surface, where the position of the buried landmine is slopes, is defined as area B and the ground surface, where it is the valley part of two mountains, is defined as area C.

Moreover, roughness of the ground surface is assumed to be shown in based on the roughness of the extent that the sensor head can accurately follow. The depth information $f(n_1, n_2)$ on the grid is assumed an original curved surface. Moreover the curved surface obtained from the original curved surface with the lowpass filter, the cutoff wave length 40 d_g [mm], is defined as the average curved surface $W(n_1, n_2)$. Therefore, the root-mean-square roughness R_s in the ground surface is defined as follows.

$$R_s = \sqrt{\frac{1}{(l_x / d_g + 1)(l_y / d_g + 1)} \sum_{n_1=0}^{l_x/d_g} \sum_{n_2=0}^{l_y/d_g} R^2(n_1, n_2)} \tag{13}$$

Where l_x/d_g, l_y/d_g are made to become to the integer and rough curved surface $R(n_1, n_2)$ is defined as follows.

$$R(n_1, n_2) = f(n_1, n_2) - W(n_1, n_2) \tag{14}$$

In this experiment, the range of the detection area is assumed to be l_x = 600 mm and l_y = 600 mm, and each parameter is assumed to be same shown in Table 4. Table 5 shows the root-mean-square roughness R_s and the depth of the buried landmine in this experiment.

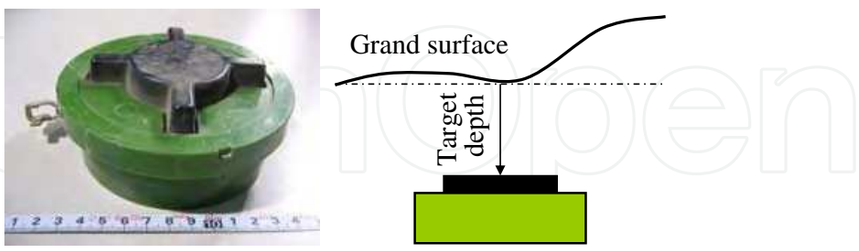

(a) PMN2 (b) Target depth

Fig. 23. Target mine

4.8.2. Experimental Result

The results of the landmine detection experiments in each detection area were shown in Fig. 24-29. In these figures, the processed outputs of the metal detector were plotted at the trajectory of the center of the sensor head's bottom.

The larger absolute values of the outputs showed that the distances between the sensor head and the buried landmines were shorter.
Moreover, the estimated positions of the buried landmines in each detection area by the method of the description in section 4.7, were shown in Table 6. In addition, in Table 7, these values were the integrated absolute values of the outputs of the metal detectors at the detection time to show the effectiveness of the gap and attitude control. Where relative values were indicated, in which the values of Case 3 were assumed 100.

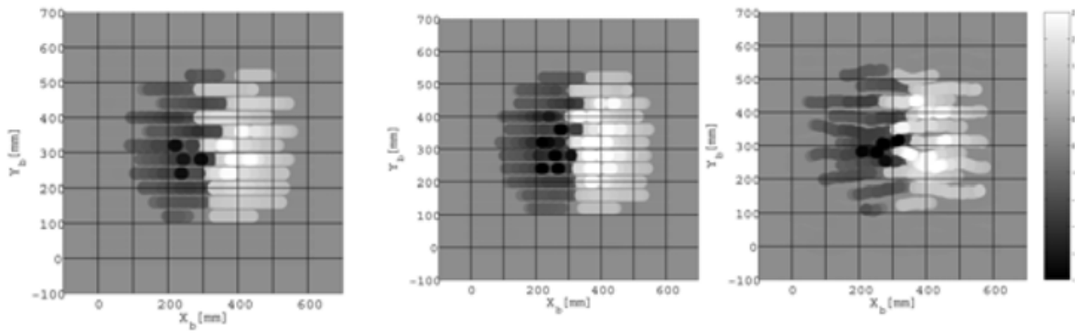

(a) Case 1 (b) Case 2 (c) Case 3

Fig. 24. Area A_1

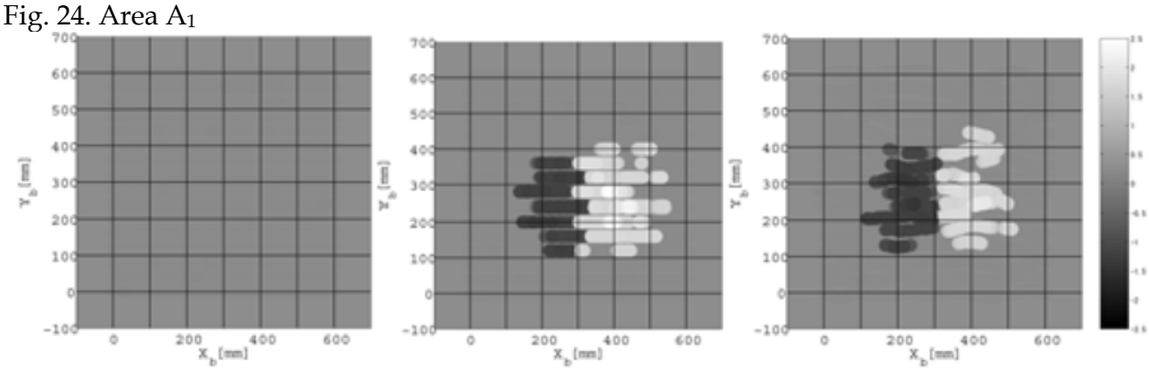

(a) Case 1 (b) Case 2 (c) Case 3

Fig. 25. Area A_2

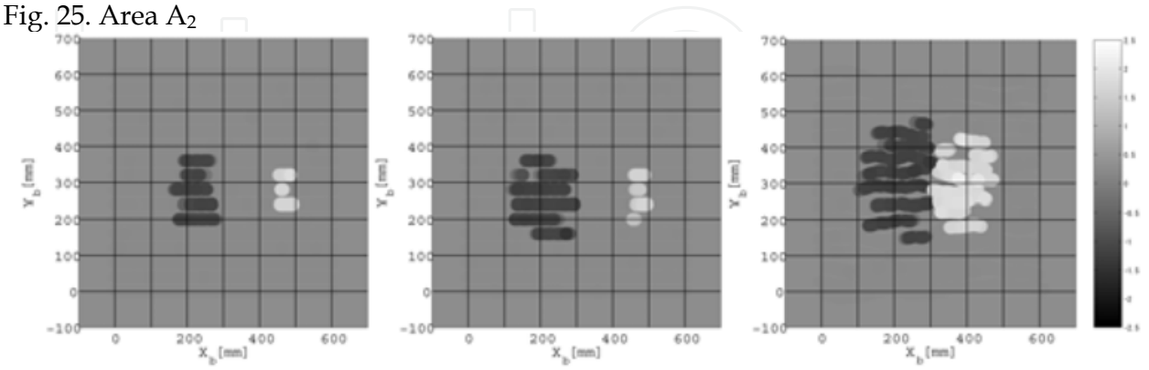

(a) Case 1 (b) Case 2 (c) Case 3

Fig. 26. Area B_1

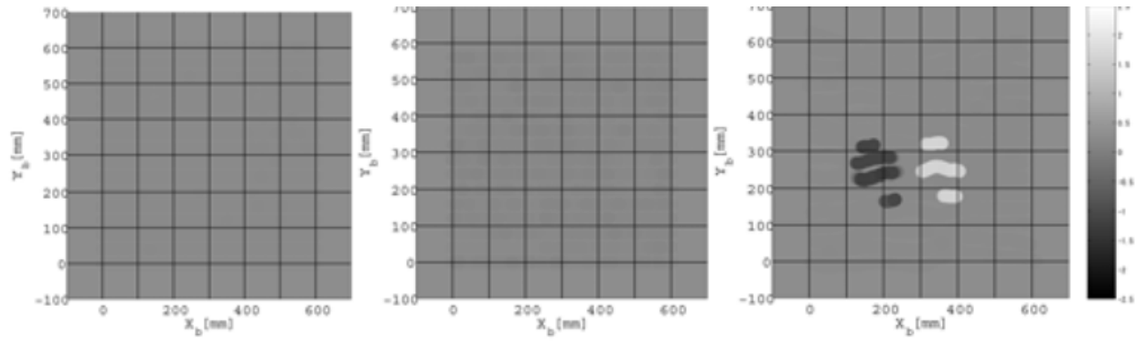

(a) Case 1 (b) Case 2 (c) Case 3

Fig. 27. Area B_2

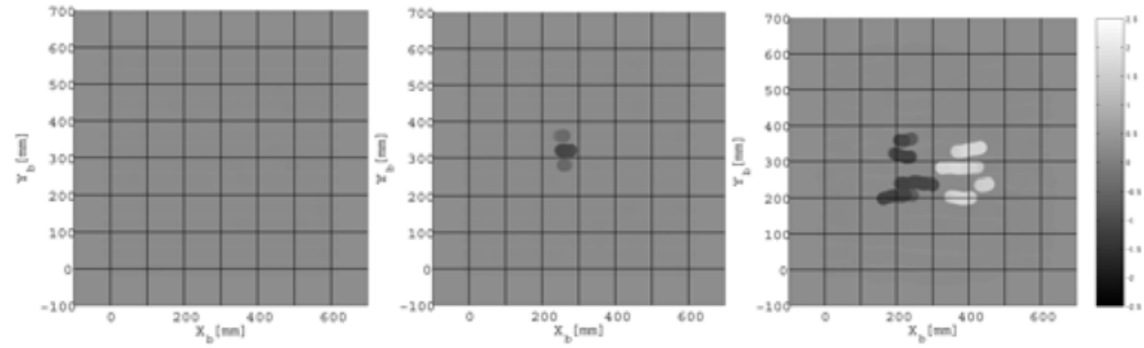

(a) Case 1 (b) Case 2 (c) Case 3

Fig. 28. Area C_1

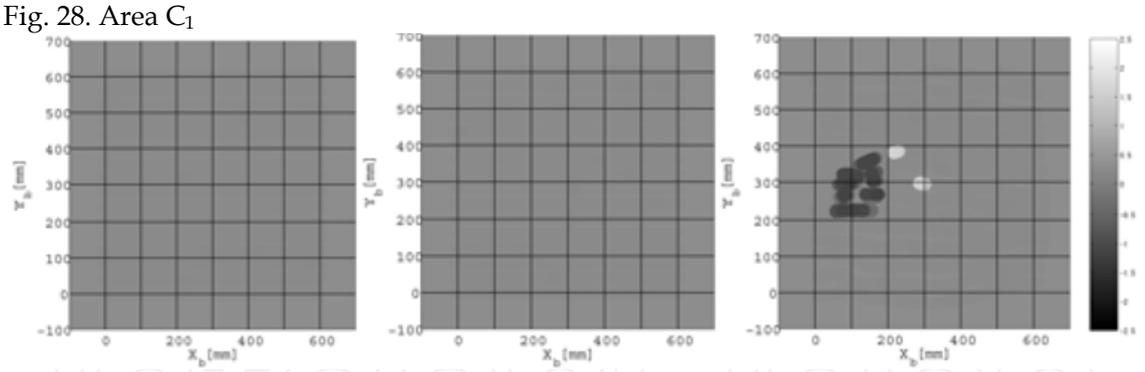

(a) Case 1 (b) Case 2 (c) Case 3

Fig. 29. Area C_2

Detection Area	Roughness(RMS)[mm]	Depth[mm]
Area A_1	8.5	50
Area A_2	8.9	120
Area B_1	9.2	120
Area B_2	10.7	120
Area C_1	10.4	120
Area C_2	11.5	120

Table 5. Specifications of detection area

[x,y]	Case 1	Case 2	Case 3
Area A_1	[322.5,315.5]	[324.1,321.1]	[319.9,321.4]
Area A_2	NaN	[310.3,252.6]	[319.1,272.1]
Area B_1	[337.5,280.7]	[344.1,259.9]	[309.3,312.6]
Area B_2	NaN	NaN	[263.7,250.7]
Area C_1	NaN	[270.7,319.4]	[312.9,270.3]
Area C_2	NaN	NaN	[192.7,310.2]

Table 6. Estimated position of landmine

	Case 1	Case 2	Case 3
Area A_1	92.5	97.0	100
Area A_2	1.4	96.5	100
Area B_1	24.0	36.1	100
Area B_2	7.4	21.8	100
Area C_1	7.8	14.7	100
Area C_2	8.4	8.4	100

Table 7. Numerical integration value of metal detector

4.8.3. Discussion

In the detection areas except Area A_1 where the depth of buried landmine is shallow, the metal reactions of Case 1 without the gap and attitude control are small, so the landmine detection performance is obviously inferior. It is clear that the gap control of the sensor head is necessary and indispensable in mine detection robots.

In the following, Case 2 and Case 3 are considered. The attitude change in Case 3 is small in a smooth ground surface, so the difference in the detection performance according to two methods, is small as shown in Fig. 24, Fig. 25 and Table 7. The buried position of both Case 2 and Case 3 can be estimated with good accuracy.

If the roughness of the slope is small, the result of Case 3 resembles a metal reaction in a smooth ground surface as shown in Fig. 26. Because the sensor head becomes parallel on the slope in Case 3.

When the ground surface is rough as shown in Fig. 27-29, the metal reaction is lost in Case 2 that is not able to change the attitude. While the metal reaction is clear in Case 3. It is shown to be able to estimate the position of the buried landmine.

As for this result, effectiveness of the gap and attitude control to the landmine detection performance is clearly shown also in Table 7. However, the error is greatly caused in the estimated position of the buried landmine according to the result of Area C_2. Because the gap is greatly caused at the center of the sensor head's bottom, when the attitude angle grows. It is a disadvantage in the attitude control.

4.9 Conclusions

In the present investigation the development of a Controlled Metal Detector (CMD) for controlling the gap and attitude of the sensor head has been presented. The trajectory planning of the sensor head with 3-D stereovision has been carried out for controlling the gap and attitude of the sensor head to the ground surface. The safety margins considered during the development of the trajectory planning algorithm makes it robust against any accidental collision of the sensor head when it is intended to scan an uneven mine affected

area. The trajectory planning algorithm makes all efforts to control the gap and attitude of the sensor head such that it follows the uneven ground surface that is conducive for the mine detection by the metal detector. The experimental results presented in this paper exhibit the effectiveness of the CMD for buried landmine detection over uneven ground.

5. Control and Operational of a Teleoperated and Master-Slave Hydraulic Manipulator for Landmine Prodding and Excavation

The focus of the MHV, shown in Figs.7 and 8, has since shifted to being primarily a sensor platform. A high landmine detection rate was the foremost goal of the JST project, and the importance of sensing is evident in the number of sensing robots that have been developed in recent years, but the fact remains that the majority of demining accidents occur during prodding, where deminers do the work manually with a prod or knife, and a little fatigue or momentary breach of SOP can be disastrous. To eliminate the personal risk inherent in prodding, there is need for a small machine that can prod where sensors have detected a possible mine in situations where large flail machines cannot be used.

The aim of this work is to develop a practical machine that can be readily put to work in the field. It is being developed with the following key considerations:

- The machine should be easy to use, with a simple and intuitive user interface; the operator should not require a lot of training time to become proficient.
- It should maintain a speed comparable to manual prodding.
- It should be robust and reliable.

The complete system will require motion control for positioning the arm, and some form of force compliance control for work involving contact with the ground. The scope of this paper is limited to an overview of the system and no-contact motion control of a single joint of the arm. In this section, we first give a description of the tool arm. The envisioned typical operation is then described. Then a short description of the user interface is given along with motion reference generation.

Figure 30. shows the 6-degree-of-freedom hydraulic tool arm, from here called the manipulator. The configuration of the joints and links is shown in Fig. 31. The manipulator's end effector is equipped with a drill for breaking up hard soil, an air jet for clearing loose soil, an electromagnet for collecting small metal fragments, and a gripper for removing large rocks and other obstacles from the area of operation. The drill is vibrational rather than rotary to avoid potentially uprooting the mine or forcibly churning soil onto it thereby causing it to detonate. The manipulator is powered by a hydraulic pump and Joints 1-4 and 6 are actuated by hydraulic cylinders and Joint 5 by a hydraulic motor. Control voltages determine the current supplied to a series of valves that control the flow of fluid to the actuators. Table 8 gives the manipulator specifications. The control computer is a Pentium III PC/104 architecture system running the xPC Target real-time operating system. The control program is developed in MATLAB/Simulink on a host PC and uploaded to the control PC for execution. Angle encoders at the joints send position information to the control PC through an A/D board, and the control PC sends control voltages to the manipulator via a D/A board. Input voltages range from -5V to 5V, though at ±2V the manipulator already moves sufficiently fast. The input is therefore restricted to within ±2V. The system is highly nonlinear and the biggest obstacle to control is the input dead zone, which is explained further in later sections.

Fig.30 6-DOF hydraulic manipulator

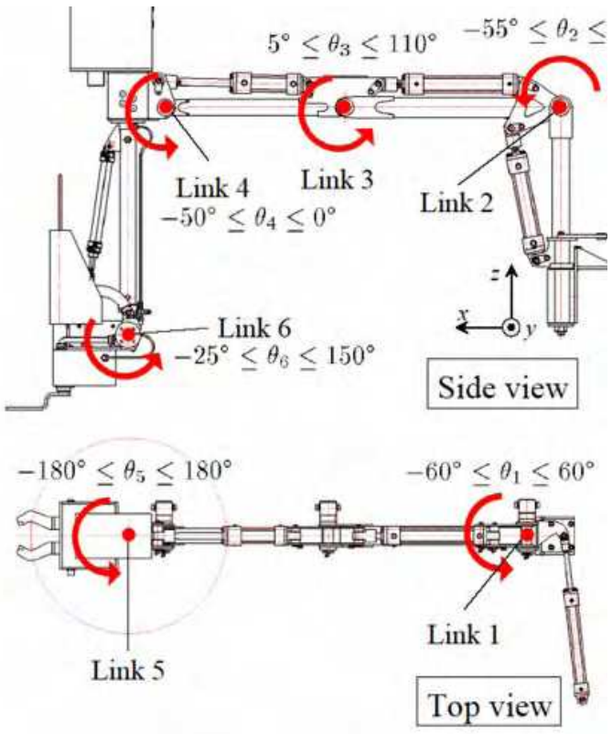

Fig.31 Configuration of manipulator

Manipulator specification

Links	Length [m]	
a_1	0.6	
a_2	0.8	
a_3	0.66	
a_4	0.14	
a_5	0.83	
Joints	Range	
j_1	±65°	Joints in Fig. 3 are at starting position 0°, clockwise is positive
j_2	-60~0°	
j_3	0~110°	
j_4	-50~0°	
j_5	±180°	
j_6	-25~160°	
Weight	200 kg	
Hydraulic Pump	13.7 MPa, 10L/min	
Air Jet	Tank Capacity: 24 m^3 Pressure: 10 MPa	

Table 8. Manipulator specification

5.1 Operation Strategy

5.1.1 Scanning Preparation – Electromagnet

The electromagnet shown in Fig.32 was originally affixed to the end effector under the assumption that the manipulator would work in tandem with a sensor arm on the same vehicle. The motivation was to clear the workspace of small metal fragments before scanning commenced in order to reduce the number of false positive sensor readings. Although the original concept of the MHV has changed (as mentioned in the introduction), a vehicle supporting both a sensor arm and a prodding arm is still the ideal scenario because the operator can switch between sensing and prodding tasks at ease without having to change out vehicles. Changing vehicles would entail extra navigation to and from the work site and great care would have to be taken to ensure the second vehicle was operating in exactly the same location as the first. Needless to say, these extra tasks would consume a great deal of time.

Provided a dual arm system is developed, either through constructing a new vehicle or redesigning the manipulator, the operation of the electromagnet is relatively straightforward. The manipulator makes and automated sweep of the area of interest with the magnet before sensing begins. The magnet collects small metal objects from the area and can release them in an out-of-the-way place. The magnet is kept close to the ground surface using gap control, which will be implemented using a 3-D map of the terrain generated by stereovision.

5.1.2 Prodding – Soil Breaker and Air Jet

A number of operation strategies are under consideration for prodding, including a master-slave system and an automated virtual reality system utilizing sensor data and a 3-D map of the terrain using stereovision. However, recalling the key considerations from the introduction, from an operator's point of view, the simplest and most intuitive strategy is joystick control of the end effector. Joystick control can be divided into two modes – large motion mode (Fig. 33a) for moving the manipulator from one area of interest to another, and small motion mode (Fig. 33b) for positioning the air jet and controlling the drill during prodding.

Precise directional control of the end effector is essential both for obstacle avoidance in large motion and prodding in small motion. Using cylindrical coordinates for the manipulator allows us to consider Joints 2-4 independently of Joints 1 and 5. Joint 1 changes the plane of operation, and Joints 2-4 determine the motion within the plane.

Once the manipulator has been positioned in the desired plane of operation, prodding can begin. If the soil is hard, the soil breaker can be used to loosen it. In keeping with time-tested safety standards, the angle of approach should be no more than 30 degrees from the surface plane. The proposed strategy requires a total of four axes of motion in small motion mode, as shown in Fig 32b. The X and Y axes and pitch are used to set the initial position the drill, and it can then be moved along its longitudinal axis into the soil. Force control will be activated when the drill makes contact with the ground so that the operator can control the strength with which the drill pushes.

The air jet can be controlled in much the same way as the soil breaker, with the same X, Y, and pitching control. When the soil has been loosened, high pressure air from the air jet clears the soil away, exposing the buried object. If the object remains covered, the process

can be repeated until the object is identified.

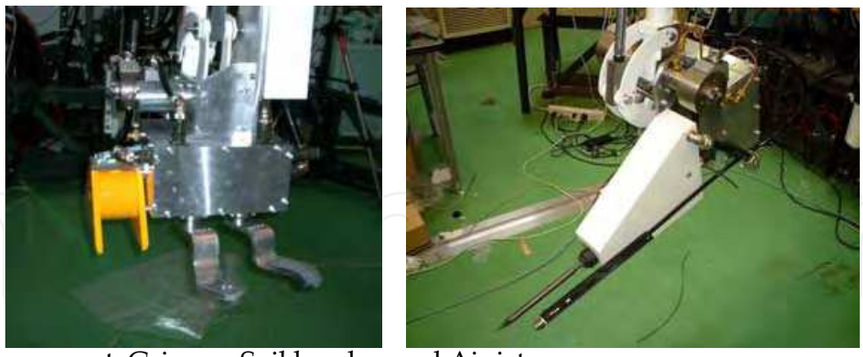

Fig. 32. Electromagnet, Gripper, Soil breaker and Air jet

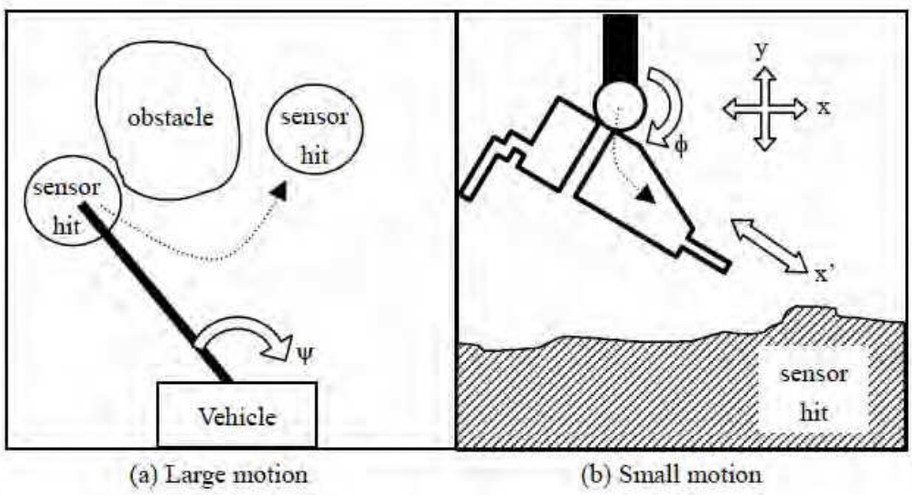

Fig. 33. Two modes of joystick manipulator control

5.2 Master-Slave Manipulator

The teleoperated and master-slave manipulation for landmine prodding and excavation is one of the important technologies in robotics based humanitarian demining. Especially, it will be highly desired to develop a completely autonomous robot which can work without any aid of the deminer in future. However, with the present state of technologies, it is not possible to develop a complete autonomous prodding and excavation robot. Therefore, the teleoperation technologies for the robots with high levels of autonomy become very important. Currently, the technologies where a deminer teleoperates a manipulator from within a safety area are not in practical use yet, like prodding and excavation. For this reason, we have developed the technologies for the teleoperated prodding and excavation of humanitarian demining robots from the safety area for the future demining missions. Figure 34 shows the master arm and the slave arm. It seems that the performance of the master-slave system is very good from Fig.35.

(a) Master Arm (b) Slave Arm

Fig. 34. Master and slave arm

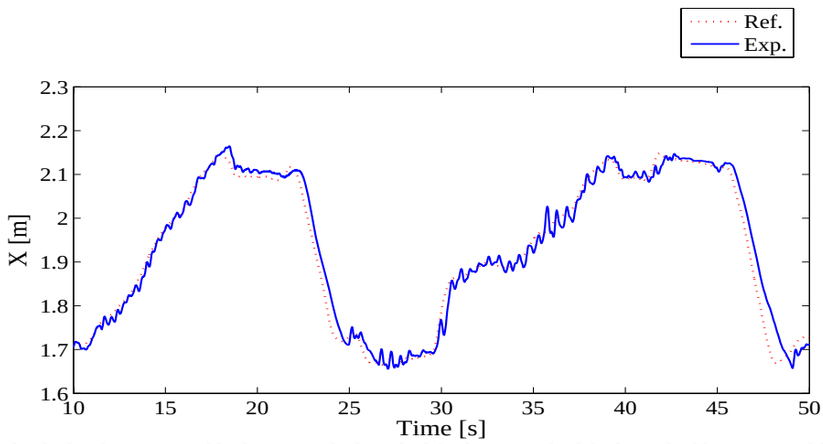

Fig. 35. Response of master-slave control (Red: Master, Blue: Slave)

6. Conclusions

The overview of mine detection robot and related technologies for humanitarina demining has been introduced. The concept which combines the flexibility of a manual system with a rapid and safer mechanized scanning of vehicle- mounted systems, with the advantage of reduced cost, size and overall system complexity. A simplified prototype was built which used a metal detector and GPR to demonstrate the concept. This system uses 3D stereo vision camera to recognize terrain profile which is used to control the trajectory of the metal detector head and GPR. Although the basic concept was successfully demonstrated. a

number of deficiencies were apparent. Further development of the system is required before it becomes ready for practical deployment. Planned future work includes the following; (1)In the present implementation, detector and GPR data and poison information are referred to a co-ordinate system fixed to the vehicle. In the future, vehicle navigation information will be used to refer all measurements to an earth-fixed co-ordinate system. (2)The detection rate in the outdoor test field should be much higher than a manual operation. (3)Also, the detection speed should be much faster than a manual operation.

7. References

Armada, M.A. et al. (2005), Configuration of a legged robot for humanitarian de-mining activities, *Proceedings of the IARP International Workshop on Robotics and Mechanical Assistance in Humanitarian Demining (HUDEM2005)*, Tokyo, Japan, (2005-6), pp. 131-135

Baudoin, Y. et al. (2000), Humanitarian Demining and Robotics State-of-the art, Specifications, and On-going Research Activities, *Proceedings of the Third International Conference on Climbing and Walking Robots (CLAWAR2000)*, Mdrid, Spain, (2000-10), pp. 869-877, ISBN: 1860582680

Baudoin, Y: CD-ROM of Proceedings of the Mine Actions, Royal Military Academy, 18-19 April, 2002

Chesney, R. et al. (2002), Terrain Adaptive Scanning of Conventional Mine Detectors, *Proceedings of the IARP International Workshop on Robotics and Mechanical Assistance in Humanitarian Demining (HUDEM'02)*, (2002-11), pp. 69-73

Clark, F. et al. (2007), Visual terrain mapping for Mars exploration, *Computer Vision and Image Understanding*, Vol. 105, No.1, (2007-1), pp. 73-85, ISSN: 10773142

Claudio, B. et al. (1998), Ground penetrating radar and imaging metal detector for antipersonnel mine detection, *Journal of Applied Geophysics*, Vol. 40, No.1-3, (1998-10), pp. 59-71, ISSN: 09269851

Das, Y., K.Russell, N.Kircanski and A.A. Goldenberg: An articulated robotic scanner for mine detection: a novel approach to vehicle mounted systems, Proc. SPIE Conference on Detection and Remediation Technologies for Mines and Mine-like Targets IV. Vol.3710, Orlando, FL, USA, 5-9 April, 1999.

Demining Technology Center, http://diwww.epflch/w3lami/detec/rodemine.html

Geneva International Center for Humanitarian Demining: Mechanical Demining Equipment Catalogue,pp.22-25,2002

ibid, pp.130-133, 2002

Homayoun, N. et al. (2007), Real-time motion planning of an autonomous mobile manipulator using a fuzzy adaptive Kalman filter, *Robotics and Autonomous Systems*, Vol. 55, No.2, (2007-2), pp. 96-106, ISSN: 09218890

Iwasaki, M. et al. (2003), High Accuracy Position Control Method for Robot Manipulator Using Positon-Based Stereo Visual Servoing, *Transactions of the Japan Society of Mechanical Engineers. C*, Vol. 69, No.681, (2003-5), pp. 1323-1329, ISSN: 03875024 (In Japanese)

James Madison University, Mine Action Information Center, Journal of Mine Action, James Madison University, http://maic.jmu.edu/

Japan Sience and Technology Agency: http://www.jst.go.jp/

Kase, H. et al. (1993), Manipulator Control by Visual Servoing with Stereo Vision, *Transactions of the Institute of Systems, Control and Information Engineers*, Vol. 6, No.8, (1993-8), pp. 360-367, ISSN: 13425668 (In Japanese)

Kenneth, M. et al. (1998), The detection of buried landmines using probing robots, *Robotics and Autonomous Systems*, Vol. 23, No.4, (1998-6), pp. 235-243, ISSN: 09218890

Kopacek,P.: A "TOOL KIT" for Demining Robots, Proceedings of the IARP Workshop on Robots for Humanitarian Demining (HUDEM'02), pp.105-110, November 3-5, 2002

Nicolas, V. et al. (2002), Qualitative evaluation of computer vision algorithms in polar terrains, *Robotics and Autonomous Systems*, Vol. 40, No.2-3, (2002-8), pp. 139-149, ISSN: 09218890

Nonami, K. et al. (2003), Development and Control of Mine Detection Robot COMET-II and COMET-III, *JSME International Journal, Series C*, Vol. 46, No.3, (2003-9), pp. 881-890, ISSN: 13447653

Nonami,K.,Aoyama,H., Research and Development of Mine Hunter Vehicle for Humanitarian Demining, Proceedings of the IARP International Workshop on Robotics and Mechanical Assistance in Humanitarian Demining (HUDEM'05), pp.76-81, 2005

Rochaa, R. et al. (2005), Cooperative multi-robot systems: A study of vision-based 3-D mapping using information theory, *Robotics and Autonomous Systems*, Vol. 53, No.3-4, (2005-12), pp. 282-311, ISSN: 09218890

Shao, H., Nonami K., Wojtara, T., et al., Neuro-Fuzzy Position Control of Demining Tele-Operation System Based on RNN Modeling, Robotics and Computer-Integrated Manufacturing, Vol. 22, Issue 1, pp. 25-32, Feb., 2006.

US,DoD Humanitarian Demining R&D Program, Humanitarian Demining, Developmental Technologies 2000-2001

Viesti, G. et al. (2007), The detection of landmines by neutron backscattering: Exploring the limits of the technique, *Applied Radiation and Isotopes*, Vol. 64, No.6, (2006-6), pp. 706-716, ISSN: 09698043

Xiao, D., et al. (2004), Real-time integration of sensing, planning and control in robotic work-cells, *Control Engineering Practice*, Vol. 12, No.6, (2004-6), pp. 653-663, ISSN: 09670661

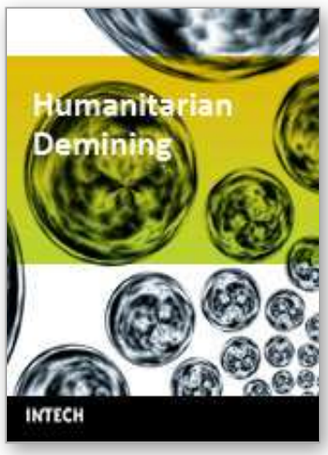

Humanitarian Demining

Edited by Maki K. Habib

ISBN 978-3-902613-11-0
Hard cover, 392 pages
Publisher I-Tech Education and Publishing
Published online 01, February, 2008
Published in print edition February, 2008

United Nation Department of Human Affairs (UNDHA) assesses that there are more than 100 million mines that are scattered across the world and pose significant hazards in more than 68 countries. The international Committee of the Red Cross (ICRC) estimates that the casualty rate from landmines currently exceeds 26,000 persons every year. It is estimated that more than 800 persons are killed and 1,200 maimed each month by landmines around the world. Humanitarian demining demands that all the landmines (especially AP mines) and ERW affecting the places where ordinary people live must be cleared, and their safety in areas that have been cleared must be guaranteed. Innovative solutions and technologies are required and hence this book is coming out to address and deal with the problems, difficulties, priorities, development of sensing and demining technologies and the technological and research challenges. This book reports on the state of the art research and development findings and results. The content of the book has been structured into three technical research sections with total of 16 chapters written by well recognized researchers in the field worldwide. The main topics of these three technical research sections are: Humanitarian Demining: the Technology and the Research Challenges (Chapters 1 and 2), Sensors and Detection Techniques for Humanitarian Demining (Chapters 3 to 8), and Robotics and Flexible Mechanisms for Humanitarian Demining respectively (Chapters 9 to 16).

InTech Europe
University Campus STeP Ri
Slavka Krautzeka 83/A
51000 Rijeka, Croatia
Phone: +385 (51) 770 447

InTech China
Unit 405, Office Block, Hotel Equatorial Shanghai
No.65, Yan An Road (West), Shanghai, 200040, China
中国上海市延安西路65号上海国际贵都大饭店办公楼405单元
Phone: +86-21-62489820

Fax: +385 (51) 686 166
www.intechopen.com

Fax: +86-21-62489821

IntechOpen